Cellulose (2021) 28:4685–4700
https://doi.org/10.1007/s10570-021-03829-3

ORIGINAL RESEARCH

Scalable coating methods for enhancing glass fiber–epoxy interactions with cellulose nanocrystals

Ejaz Haque · Shadi Shariatnia · Tae-Joong Jeong · Dorrin Jarrahbashi · Amir Asadi · Tequila Harris · Robert J. Moon · Kyriaki Kalaitzidou

Received: 5 January 2021 / Accepted: 11 March 2021 / Published online: 24 March 2021

Abstract Two scalable coating techniques, slot die and spray coating (SC), are used to apply cellulose nanocrystals (CNCs) to the surface of glass fibers with the goal of enhancing interfacial interactions between glass fibers and epoxy and, consequently, the strength of fiber-reinforced composites. The quality of the cellulose coatings and the interfacial shear strength, assessed via the single fiber fragmentation test, are determined as a function of the method and conditions used to coat the fibers. In addition, a comparison with glass fibers coated with identical CNC formulations using a laboratory-scale dip coating (DC) technique is provided. Results from both scalable methods were found to be comparable or superior to the DC technique, with SC outperforming DC by up to 18% on average depending on the coating applied. Further analysis was conducted on coating morphology, fracture behavior, elemental composition, and surface loading. The observed differences can be used to determine which technique is most appropriate for a given application. This work demonstrates the viability in adapting existing, scalable processes for CNC

Supplementary Information The online version contains supplementary material available at https://doi.org/10.1007/s10570-021-03829-3.

E. Haque (✉) · K. Kalaitzidou
School of Materials Science and Engineering, Georgia Institute of Technology, Atlanta, GA 30332, USA
e-mail: ehaque3@gatech.edu

K. Kalaitzidou
e-mail: kyriaki.kalaitzidou@me.gatech.edu

S. Shariatnia · D. Jarrahbashi
J. Mike Walker '66 Department of Mechanical Engineering, Texas A&M University, College Station, TX 77843-3123, USA
e-mail: shadishariatnia69@tamu.edu

D. Jarrahbashi
e-mail: djarrahbashi@tamu.edu

T.-J. Jeong · T. Harris · K. Kalaitzidou
George W. Woodruff School of Mechanical Engineering, Georgia Institute of Technology, Atlanta, GA 30332, USA
e-mail: tjeong7@gatech.edu

T. Harris
e-mail: tharris3@gatech.edu

A. Asadi
Department of Engineering Technology and Industrial Distribution, Texas A&M University, College Station, TX 77843-3367, USA
e-mail: amir.asadi@tamu.edu

A. Asadi
Department of Materials Science and Engineering, Texas A&M University, College Station, TX 77843-3367, USA

glass fiber coatings and establishes key avenues for future process optimization.

Keywords Cellulose nanocrystals · Slot die coating · Spray coating · Composites · Fiberglass · Interphase

Introduction

Glass fiber-reinforced composites (GFRCs) are among the most commonly studied and manufactured materials for various applications including automotive due to their low cost and high production volumes (Güler et al. 2018; Huber et al. 1980; Lagel et al. 2016; Reichwein et al. 2010). The main challenge is their low mechanical performance compared to steel (Energy 2016), which has inspired research on enhancing GFRC properties to meet structural standards. Nanomaterials have shown promise in improving stiffness and strength of GFRCs, such as cellulose nanocrystals (CNCs) that have been shown to enhance fiber-matrix interactions when applied to the fiber surface (Asadi et al. 2016, 2017; Goffin et al. 2011). Additionally, they are highly abundant in nature, exhibit high mechanical properties and low densities, and their cost is projected to drop as global production expands over the next several years (de Assis et al. 2017; Moon et al. 2011, 2016). However, the scalability of coating glass fibers with CNCs is still a challenge. The ideal approach would be to incorporate CNCs into the sizing applied to glass fibers by the fiber manufacturer, but similar approaches described in the literature have been limited to lab scale techniques. To facilitate the commercialization of this technology, the efficacy of CNC coatings must first be demonstrated using scalable techniques, such as slot die and spray coating.

Slot die coating is an industrially relevant technique for fabricating uniform thin films using roll-to-roll (R2R) production. Conventional slot die coating is performed by continuously pumping fluid between two parallel plates onto a moving web to form thin films. It has been used in electronics applications to coat solutions onto continuous and porous substrates with fast production rates, a high degree of control over film thickness, and minimal material waste (Ding et al. 2013; Hösel et al. 2014; Jeong et al. 2020). Dispersions of solid polymers and/or nanomaterials have also been successfully coated on continuous media such as organic solar cells (Larsen-Olsen et al. 2012). However, slot die coating of porous media with dispersions of nanomaterials such as CNCs has yet to be explored.

Spray coating is an industrially relevant technique for nanoparticle deposition in manufacturing, electronics, and energy applications (Girotto et al. 2009; Green et al. 2008; Vak et al. 2007). Twin-fluid spray coating systems use an assisting gas to atomize a fluid and direct the droplets toward the substrate (Lefebvre 1992). Air-assisted atomizers can produce micron-sized droplets with narrow size-distribution along the cross-sectional area of the spray (Lefebvre 1996). These systems have been used to deposit CNCs on acrylonitrile butadiene styrene filaments to increase interlayer adhesion in 3D printed polymers (Shariatnia et al. 2019). A similar approach could conceivably be used for the coating of glass fibers for GFRC reinforcement, but this has not yet been proven.

This work investigated the viability of slot die and spray coating techniques in applying nanocellulose-based coatings on glass fibers. The single fiber fragmentation test (SFFT) was used to assess interfacial shear strength (IFSS), an indicator of composite performance. The effects of CNC concentration, dispersion medium and coating technique on IFSS were evaluated. In addition, a comparison of SFFT results between fibers coated using the scalable slot die and spray coating techniques and those coated by a dip coating method in our recent study (Goswami et al. 2019) is also provided to determine if scalable coating techniques can provide comparable performance to lab-scale ones. Coated fibers were characterized via scanning electron microscopy (SEM), X-ray photoelectron spectroscopy (XPS), and thermogravimetric analysis (TGA) to understand coating morphology, elemental composition, and fiber mass loading. Differences in these characteristics are compared to understand the specific advantages of each technique and how they may be optimized.

R. J. Moon
The Forest Products Laboratory, U.S. Forest Services, Madison, WI 53726, USA
e-mail: robert.j.moon@usda.gov

Experimental

Materials

US Composites (West Palm Beach, FL, USA) 635 thin epoxy and 556 slow amine hardener were used as the resin and curing agent respectively for fabrication of single fiber tensile coupons. The glass fibers (GFs) provided by Owens Corning (Oak Brook, IL, USA) were ME1510 multiend rovings (TEX 4800) with a 10 μm single fiber diameter. CNCs with methyl(triphenyl) phosphonium counterions were provided by the laboratory of Prof. Douglas M. Fox (American University, Washington, DC, USA) as a 4 wt.% aqueous suspension, the preparation of which has been described previously (Fox et al. 2016). As shown by Fox et al., the ion exchange process performed on these CNCs enables them to stay well-dispersed in aqueous solutions while improving their dispersity in epoxy systems similar to those used in this work (Fox et al. 2016). Pluronic P123, a poloxamer used in the preparation of the emulsions, was purchased from Sigma Aldrich (St. Louis, MO, USA).

Coating solution preparation

Coating solutions were prepared following the protocols established and reported in our prior work (Goswami et al. 2019). To highlight the relationship between coating method and fiber-matrix interfacial interactions, the best-performing coating formulation from that study was chosen for comparison with this work alongside two control coating formulations. The naming scheme used for the coated GF samples investigated in this study is as follows: the first part indicates the coating method used (i.e., DC, SD and SC for dip coating, slot die coating and spray coating respectively); the second part indicates whether a 5 wt.% epoxy emulsion (5EM) was used instead of just an aqueous solution; the third part indicates the CNC concentration in the coating formulation (1 wt.%). All formulations used in this study are described in Table 1.

Slot die coating setup

CNC solutions were placed in 20 mL NORM-JECT® sterile syringes which were then tightly clamped to a Fusion® syringe pump. A R2R system, shown schematically in Fig. 1a, was used to coat GFs adhered to an acrylic plate. A stainless-steel slot die with a width of 130 mm and a slot gap (W) of 0.1 mm was mounted on the R2R system with a coating gap (H) of 0.3 mm maintained between the GFs and the slot die opening. CNC suspensions were pumped through the slot die at a flow rate (Q) of 1 mL/min. Polyethylene terephthalate (PET) was used as a carrier web for the acrylic plates, and the velocity of the web (V) was set to 0.5 mm/s. These process parameters were determined by coating rovings at various settings until the resulting coatings exhibited similar morphologies, as observed via SEM, to dip coated samples studied in our previous work (Goswami et al. 2019). For easier processability, multiple rovings were adhered to a sacrificial acrylic plate using tape at the two ends. Rovings had at least 10 mm of space between them to ensure no overlap. After coating, samples were left in ambient conditions for at least 24 h to allow for water evaporation. TGA confirmed this 24-h period was sufficient to reduce surface water content to within 0.05 wt.%.

Spray coating setup

A schematic of the spray coating system used is shown in Fig. 1b. CNC coating solutions were delivered to the nozzle using an impeller pump (SCC Pumps Inc. IL, USA) for mixing with pressurized dry air. Solutions were continuously circulated within this system, ensuring no sedimentation occurred. The tertiary mixture then passed through a single-orifice nozzle (Spraying Systems Co., IL, USA) to generate micron-sized droplets that further evaporated and deposited nanoparticles on GFs. Rovings were attached to a flat plate, and a rail-and-motor was used to move them across the spray path such that their entire length was coated. An Arduino microcontroller board was implemented to control the speed of this movement. To establish operating conditions for fiber coating, a high-speed diffuse back illumination (i.e. shadowgraph) imaging system was used for direct visualization of jet breakup, droplet formation, particle size, spray angle, and penetration length. A Photron Fastcam SA5 camera with 21 μm resolution and a Nikon Nikkor 50 mm lens was used along with a 500-W halogen incandescent light source for back illumination. An image processing code was developed in R-Studio to subtract the background, and to adjust the contrast,

Table 1 Coating formulations used in this study and their respective labels

Sample ID	Coating method	Emulsion content	CNC content
Uncoated	N/A	N/A (aqueous)	N/A
DC 1CNC	Dip coated	N/A (aqueous)	1 wt.% CNC
SD 1CNC	Slot die coated	N/A (aqueous)	1 wt.% CNC
SC 1CNC	Spray coated	N/A (aqueous)	1 wt.% CNC
DC 5EM	Dip coated	5 wt.% emulsion	N/A
SD 5EM	Slot die coated	5 wt.% emulsion	N/A
SC 5EM	Spray coated	5 wt.% emulsion	N/A
DC 5EM 1CNC	Dip coated	5 wt.% emulsion	1 wt.% CNC
SD 5EM 1CNC	Slot die coated	5 wt.% emulsion	1 wt.% CNC
SC 5EM 1CNC	Spray coated	5 wt.% emulsion	1 wt.% CNC

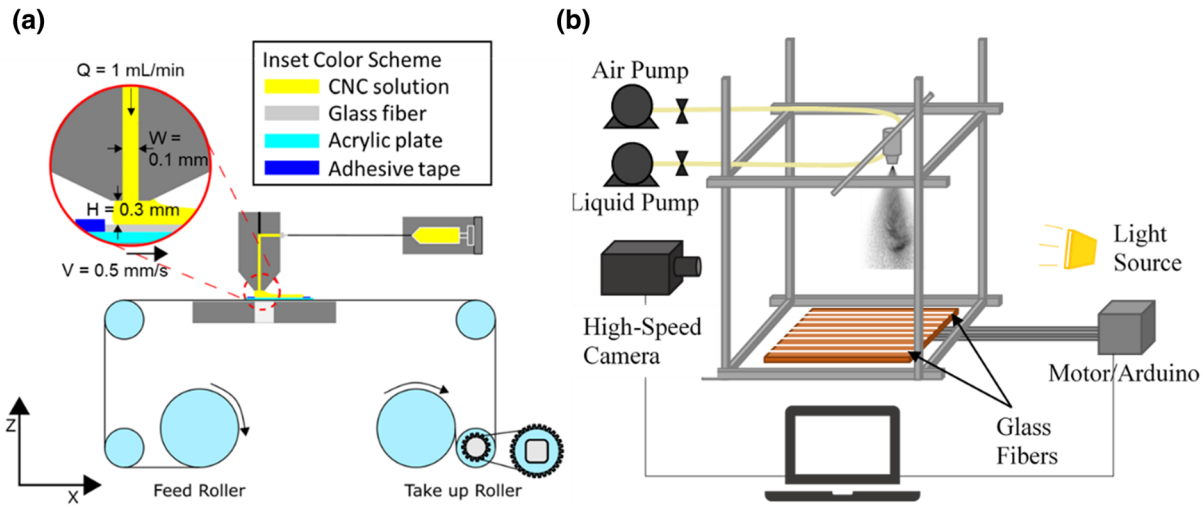

Fig. 1 Schematic of experimental setup for **a** slot die coating and **b** spray coating. Q represents the solution flow rate, W represents the gap width of the slot die, H represents the spacing between the slot die and the substrate, and V represents the velocity of the carrier web

brightness, and gamma factor of the images. Example images for the SC 1CNC formulation are depicted in Fig. 2.

To determine an appropriate atomization pressure, droplet sizes were measured from jets produced at 100 kPa and 200 kPa. The droplets yielded from these jets had comparable average diameters, independent of atomization pressure and coating formulation, which ranged from 29 to 34 μm. The lower pressure of 100 kPa was selected for this work for easier processing. Rail speed was also varied from 5 mm/s to 15 mm/s. By spray coating rovings at different speeds and evaluating fiber mass loss with TGA, a rail speed of 5 mm/s was chosen since it produced coatings with

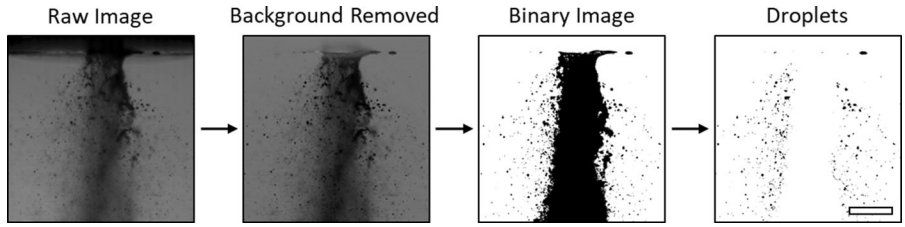

Fig. 2 Processing of jet breakup images. Frame rate = 20,000 fps. Shutter speed = 370 ns. Scale bar is 1 mm

similar masses to samples dip coated in the same formulations used in our prior study (Goswami et al. 2019). Prior to TGA, fibers were dried in ambient conditions in the same manner as slot die coated fibers.

Characterization of glass fiber surface

Coated and uncoated rovings and single fibers pulled from rovings were sputter coated with gold and imaged using a Zeiss (Oberkochen, Baden-Württemberg, Germany) Ultra 60 FE-SEM at an accelerating voltage of 5 kV. Elemental composition of coated fiber surfaces was probed using a Thermo Scientific (Waltham, MA, USA) K-Alpha X-ray photoelectron spectrometer (XPS) equipped with a 1.486 keV aluminum K-alpha x-ray source. Samples were probed for carbon (C), oxygen (O), nitrogen (N), silicon (Si), sulfur (S), and phosphorous (P). Mass of coating adhered to the fiber surface was determined by heating 10–20 mg samples of chopped coated rovings to 600 °C at a rate of 10 °C/min under nitrogen atmosphere using a TA Instruments (New Castle, DE, USA) Q50 TGA. Mass loss from this process is reported as an average of three samples.

Characterization of glass fiber–epoxy interactions

The single fiber fragmentation test (SFFT) was performed to assess interfacial shear strength (IFSS), a measurement of fiber-matrix adhesion. Test samples consisted of a single glass fiber embedded in a dogbone-shaped epoxy coupon. The mixing of the two part resin system and the curing conditions were adapted from our prior study (Goswami et al. 2019). In the current work, the fiber coating procedures coat the entire roving, and single fibers used in SFFT sample preparation are separated after a whole roving is coated.

SFFT requires coupons to be loaded continuously until they reach fracture saturation, the point at which stress transfer between the fiber and matrix is no longer sufficient to fracture the fiber. To determine when saturation is achieved, specimens were tested at a constant extension rate of 1 mm/min until crosshead extensions of 3, 4, and 5 mm were reached. The mean number of fragments observed after testing was approximately equal in all cases, suggesting that saturation is achieved by an extension of 3 mm for the coatings described in this work.

Fragmentation behavior was studied using a Leica DM2500p cross-polarized optical microscope to count fracture events along the sample gauge length. The number of fractures was used as a surrogate for IFSS since the two values are directly related and other existing methods to calculate IFSS are non-universal (Goswami et al. 2019). Cross polarizers were used to visualize birefringent behavior surrounding fractures to further understand the effect of coatings on local interphase strength.

Results and discussion

Coatings on the GF surface

Coating morphology

Coated rovings and single fibers removed from the coated rovings were imaged by SEM to assess the effect of fiber separation on coating quality. For each formulation, images of the top and bottom sides of the rovings were taken. Figure 3 illustrates differences in surface morphology before and after coating with the SD method. Notable features on the uncoated rovings include patches of the GF sizing on their surfaces and between individual fibers, as well as occasional dust particles. The sizing layer was left intact on all samples, as removing it introduces surface defects. Neither the coating nor curing processes were found to damage the sizing. Analysis of fracture surfaces from our previous work reflects the presence of sizing on the surfaces of fibers in cured composites, and TGA experiments performed in the current study (see Fig. 7) showed that sizing remained on all GF surfaces after the applied coating layer was removed (Asadi et al. 2017). All coating formulations described in this work were thus applied directly on top of the sizing layer, which remained intact in all of the following SEM images.

The SD 5EM formulation completely covered the GF sizing layer and encapsulated pre-existing contamination. Spaces between the fibers filled with the liquid coating formulation, largely eliminating the contour of the roving stemming from the cylindrical geometry of individual fibers. This contour remained distinguishable on the bottom face, suggesting that the coating layer was thinner or nonexistent on the bottom of the roving. This was likely a consequence of limited

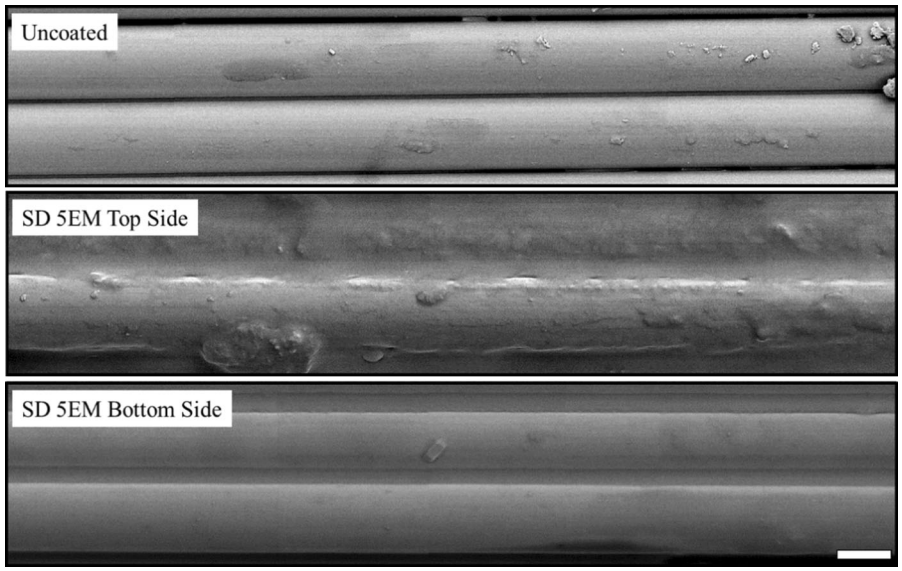

Fig. 3 SEM images of an uncoated fiber roving and the top and bottom sides of a roving slot die (SD) coated in 5 wt.% emulsion (5EM). Scale bar is 10 μm

penetration of the coating formulation through gaps in the layers of sizing between the fibers. However, XPS was used to confirm that the bottom side was successfully coated, and the results of this test are further described in Section "Chemical Species on Coated Roving Surfaces".

GFs coated with the SC 5EM formulation exhibited different surface morphology compared to GFs coated in the SD 5EM formulation. Unlike the SD 5EM samples, the top and bottom sides of the SC 5EM samples were visually similar, suggesting that the thickness of the coating layer was more uniform. The coating layer also displayed nanoscale cracking, and this phenomenon was particularly noticeable in areas of contact between the coating layer and the GF sizing as shown in Fig. 4. No such cracks were observed upon similar high-magnification analysis of SD coated samples. This cracking behavior may thus be related to differences in solution deposition between the SD and SC processes. In SD, when the coating is constrained between the slot die lip and the substrate, penetration of solution between the fibers is governed by pressure-driven flow and capillary forces. However, after the substrate moves and the solution is no longer confined by the slot die head, further penetration is driven exclusively by capillary forces (Ding et al. 2016). Low pressures and weak capillary forces may have led to the lower degree of penetration observed for SD

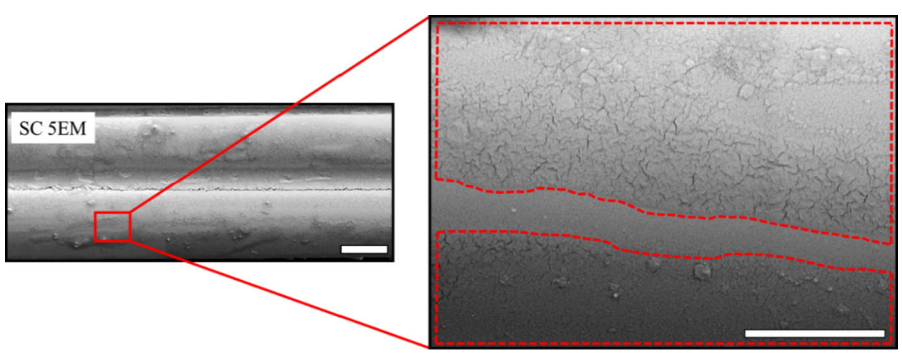

Fig. 4 SEM image of the top side of a roving spray coated (SC) in 5 wt.% emulsion (5EM). Boxes highlight areas of contact between sizing and coating where coating cracked. Scale bars are 10 μm for left image and 5 μm for inset

samples compared to SC samples, as the latter were coated with a pressurized spray. This may in turn have led to a lower volume of liquid on the top surface of SC rovings, resulting in a thinner coating more susceptible to cracking. Crack formation is also strongly influenced by the physical structure of the film, suggesting that SD and SC may have yielded different coating structures that led to different cracking behavior. Evidence to support this notion is further discussed in Section "Mass of Coating on the Fiber Surface".

Certain coating type and method combinations resulted in non-uniform coating layers. The most extreme example was the SD 1CNC formulation. During the coating process, the liquid layer tended to pool toward the sides of the rovings rather than remain evenly spread across the entire surface. This resulted in morphologies such as those shown in Fig. 5, wherein parts of the roving were covered in a thick, cake-like film while others exhibited no visible coating. XPS analysis confirmed that the regions with no visible deposits were actually coated in a thin layer of CNCs, showing that the coating formulation came into contact with the entire roving surface but was poorly distributed. This inhomogeneity is likely attributable to the water content of the 1CNC formulation. In SD coating, formation of a stable coating bead that can be spread evenly across the substrate surface requires balancing parameters such as deposition rate and the viscosity of the coating solution. Achieving stability at low viscosities is challenging, as it requires impractically low deposition rates or the application of external vacuum (Ding et al. 2016). At an industrial scale, investment in a vacuum system may be worthwhile if a low viscosity formulation is found to perform exceptionally well. However, the results of our DC study showed that emulsion-based coatings performed better than the lower viscosity 1CNC formulation (Goswami et al. 2019). It was thus concluded that improving homogeneity of the SD 1CNC coating may be possible but beyond the scope of the current study.

The effects of separating single fibers from coated rovings for SFFT sample preparation were investigated, and examples of separated fibers are shown in Fig. 6. The most prevalent features in each are the remnants of coating torn away from adjacent fibers. To eliminate the possibility that these features were artifacts such as contamination, the SD 5EM sample was only partially separated to capture the state of the coating layer during the separation process. Tearing of the coating layer and exposure of the base fiber are apparent in this sample. This suggests that the jagged films observed on slot die and spray coated single fibers were sections of coating torn away from neighboring fibers.

Single fibers removed from SC rovings exhibited some similar characteristics to single fibers removed from SD coated rovings. In both cases, the 1CNC formulation produced a thin, flake-like morphology while the 5EM formulation yielded a more continuous coating layer. The epoxy content in the emulsions likely increased their wettability on the GF surface due to compatibility with the aminosilane sizing. High wettability facilitates high GF surface coverage, maximizing the interfacial area of emulsion coatings and thus their ability to enhance the fiber-matrix interphase.

Aggregate formation was also found to differ between coating methods. Large solid aggregates that differed in size and shape from atmospheric contamination were occasionally observed on GFs coated in the SC 5EM 1CNC formulation. These aggregates were not found on SD 5EM 1CNC samples, suggesting that differences in coating mechanism, such as pressurization of the coating liquid in SC, may have been the cause. Small aggregates were also observed on SC 5EM samples but not DC or SD 5EM samples, providing further evidence that the atomization process can lead to agglomeration of solids. Incorporation

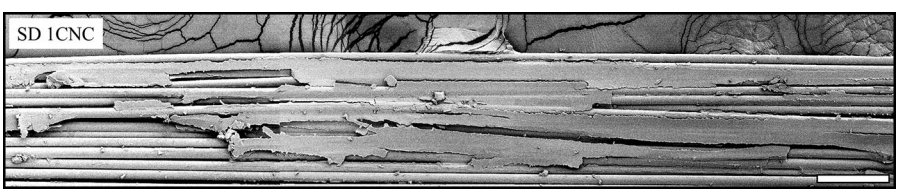

Fig. 5 SEM image of the top surface of a roving slot die (SD) coated in 1 wt.% CNC (1CNC). The area imaged is the edge of the roving, where coating solution pooled and dried unevenly. Scale bar is 100 μm

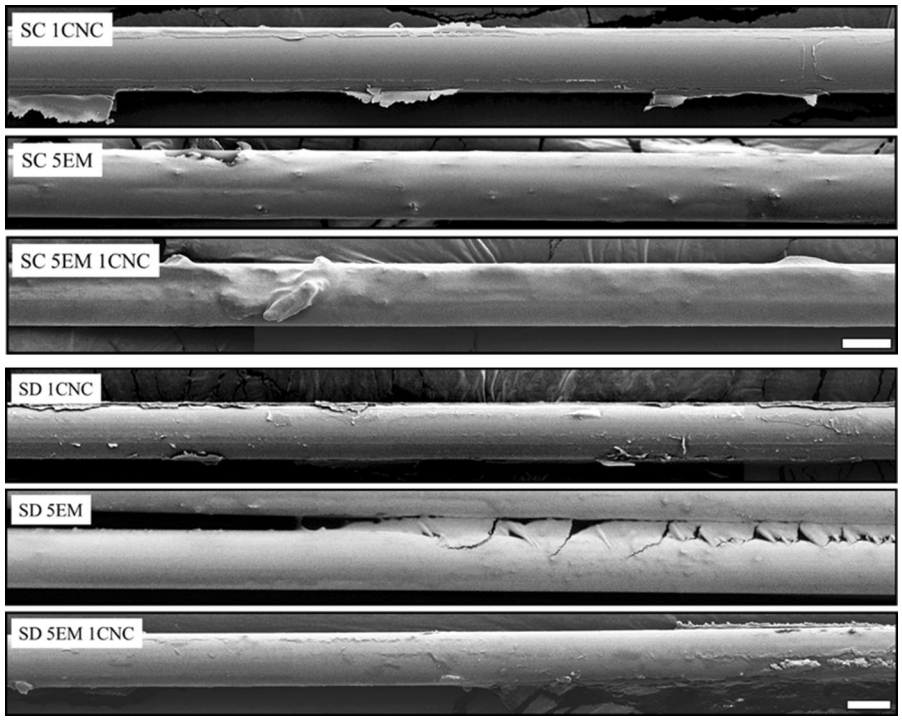

Fig. 6 SEM images of single fibers pulled from coated rovings. Rovings were slot die (SD) and spray coated (SC) in 1 wt.% CNC (1CNC), 5 wt.% emulsion (5EM), and 5 wt.% emulsion + 1 wt.% CNC (5EM 1CNC). Scale bars are 10 μm

of CNCs, a hydrophilic material with high self-affinity, may have exacerbated the size of these aggregates due to unfavorable interactions with the poloxamer.

Mass of coating on the fiber surface

The mass of coating adhered to the surface of rovings was determined using TGA, and the results are reported in Table 2. All samples were brought from room temperature to 600 °C. Changes in mass were monitored with respect to temperature, and it was observed that for all samples, mass loss plateaued at approximately 580 °C at the latest. Though 600 °C is insufficient to completely remove all organic material from the fiber surface, this plateau indicated that a stable char was achieved and this temperature could be used as a suitable basis for comparison between coatings.

As the goal of this work was to evaluate which coating methods yield the highest-quality coatings when using realistic processing conditions, this measurement was intended to assess differences in coating mass rather than confirm that each method yielded the same mass. DC samples yielded consistent results that generally tracked with the solids content of the coating solution (i.e., the mass lost for the 5EM 1CNC sample was approximately the sum of the mass lost from the 1CNC and 5EM samples individually). SC samples

Table 2 Mass (%) of coatings removed from chopped GF rovings by TGA. Averages are for 3 samples, and error is 1 standard deviation

Sample	Average mass loss (%)
Uncoated	0.8 ± 0.1
DC 1CNC	2.3 ± 0.3
SD 1CNC	4.2 ± 0.8
SC 1CNC	2.1 ± 0.3
DC 5EM	3.9 ± 0.1
SD 5EM	7.2 ± 0.6
SC 5EM	2.8 ± 0.2
DC 5EM 1CNC	6.7 ± 0.7
SD 5EM 1CNC	4.8 ± 0.03
SC 5EM 1CNC	7.1 ± 0.3

performed similarly with the exception of a slightly lower result for the 5EM coating. SD samples did not follow such clear trends, likely a consequence of coating inhomogeneity. The 1CNC solution and, to a lesser extent, the 5EM solution failed to spread evenly across the GF surface. Instead, they pooled toward the edges of rovings as previously shown in Fig. 6, resulting in sampling error that produced high averages and standard deviations for mass loss. SD 5EM 1CNC, however, exhibited very low error, reflecting the superior homogeneity of combined CNC-emulsion coatings. This difference highlights the role of solids content in achieving a stable liquid coating bead in SD coating.

In addition to total mass loss, the derivative of mass loss with respect to temperature was also studied. Figure 7 shows a comparison between SD 1CNC and uncoated GFs based on this metric, which reveals that the coated sample exhibited peaks at 320 °C and 375 °C corresponding to CNCs and sizing respectively. As previously discussed, this implies that the coating process did not result in removal of the underlying sizing. Measurements were also taken for SC 5EM 1CNC samples, which exhibited three distinct peaks at approximately 220 °C, 320 °C, and 380 °C corresponding to the decomposition temperatures of the epoxy, CNC, and copolymer (Cho et al. 2009). However, SD 5EM 1CNC samples instead yielded a single broad peak. This difference in behavior can occur due to differences in physical

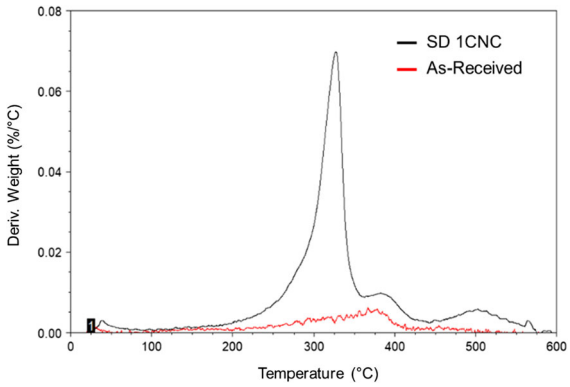

Fig. 7 Derivative of weight with respect to temperature from TGA of uncoated fibers (red) and fibers slot die (SD) coated in 1 wt.% CNC (1CNC) (black). The peak at 320 °C reflects the presence of CNCs on the coated sample, and overlapping peaks at 375 °C show that sizing remains intact on coated samples

structure at the nanoscale, such as entrapment of CNCs in a polymer network. Morphological features such as those shown in Fig. 4 provide further evidence that such differences may have been induced by mechanisms of the SD and SC processes.

Chemical species on coated roving surfaces

XPS was used to confirm the presence of CNC and/or emulsion on the fiber surface. When probing for CNCs, samples were scanned for phosphorous, a characteristic species unique to the CNC in this work due to the ion exchange process used to modify them (Fox et al. 2016). The P2p region of XPS spectra were compared between uncoated samples and CNC-coated samples, as shown in Fig. 8a. Peaks near a binding energy of 133 eV were detected for both SD and SC 1CNC, whereas the control fiber exhibited no discernible phosphorous signal. These peaks confirm that the solid deposits seen on rovings coated in the 1CNC formulation were CNCs successfully adsorbed to the surface.

Sulfur was also used as a basis for detecting CNCs due to the presence of sulfate half ester groups on their surface. For the 1CNC formulation, similar results were yielded whether using phosphorous or sulfur as a basis. However, sulfur was useful for detecting CNCs in emulsion-based coatings due to the higher atomic percentage of sulfur in the CNC structure compared to phosphorous. Figure 8b compares S2p signals from all SD coated samples. The results show peaks only for the formulations containing CNCs (SD 1CNC and SD 5EM 1CNC), showing that CNCs can be detected even when the coating layer is primarily emulsion by weight. Additionally, the lack of a sulfur peak in the SD 5EM curve confirms that sulfur is only detected when CNCs are present. Measurements were taken at multiple spots along the roving length to assess coating uniformity. Equivalent SD and SC formulations yielded peaks at approximately the same binding energies, but the range of peak intensities was slightly higher for SC samples. This provides evidence that shear forces in SD coating can, to an extent, facilitate nanoparticle distribution.

XPS was also used to detect emulsions, which aided in determining if SD 5EM rovings exhibited any coating on their bottom side (see Fig. 3). Carbon was selected as the basis for this comparison, as it is the most abundant species in the epoxy and poloxamer

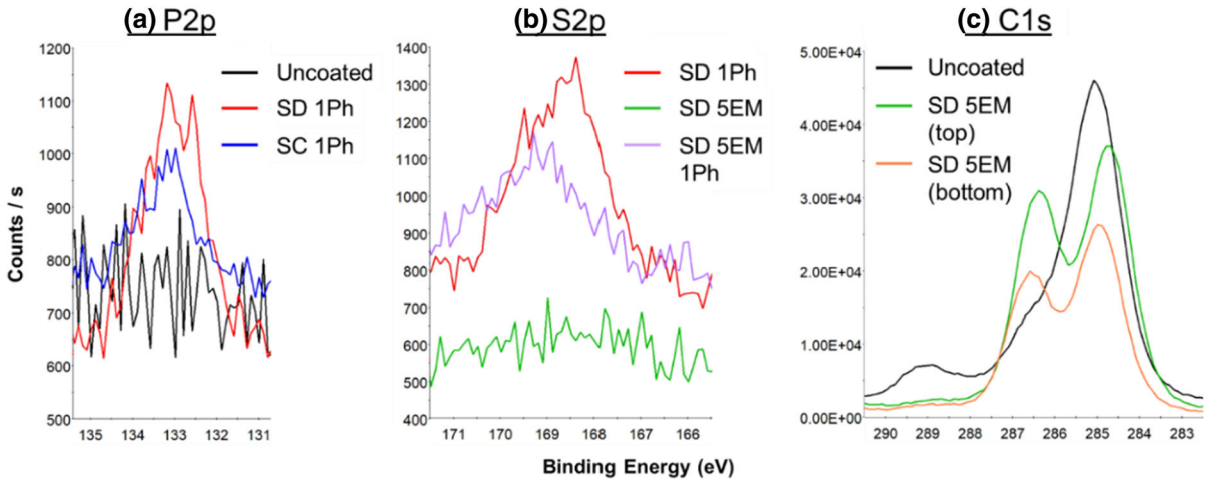

Fig. 8 Comparison of various representative regions of XPS spectra. **a** P2p region for uncoated rovings, rovings slot die (SD) coated in 1 wt.% CNC (1CNC), and rovings spray coated (SC) in 1 wt.% CNC (1CNC); **b** S2p region for rovings spray coated (SC) in 1 wt.% CNC (1CNC), 5 wt.% emulsion (5EM), and 5 wt.% emulsion + 1 wt.% CNC (5EM 1CNC); **c** C1s region for bottom and top sides of rovings slot die (SD) coated in 5 wt.% emulsion (5EM)

structures. The results in Fig. 8c show identical patterns for the top and bottom sides of the SD 5EM rovings, with prominent peaks at 286.5 eV corresponding to O-C-O bonds that are not seen in the uncoated roving. Given that no energy was supplied to the system during the coating process, it is unlikely that new covalent bonds were formed between the emulsion and the GF surface. Instead, these signals likely stemmed from the O–C–O bonds within the epoxy and poloxamer structure. This result thus suggests that coatings physically adsorb onto the GF surface, and it confirms that the coating formulation reaches the bottom side of the fiber.

Effect of CNC coatings on glass fiber–epoxy interactions: single fiber fragmentation test (SFFT)

Interfacial enhancement as a product of coating type and coating method is shown graphically in Fig. 9. This enhancement is generally reported in the literature in terms of IFSS, which is often calculated using the Kelly-Tyson model (Kelly and Tyson 1965). In this model, IFSS is a function of fiber diameter, the critical length of the fiber (i.e., its length at saturation), and the strength of the fiber at its critical length. The critical fiber length is itself dependent on the number of fiber fractures generated during SFFT and a correction factor K'. Due to the lack of a universal method for determining the critical fiber strength,

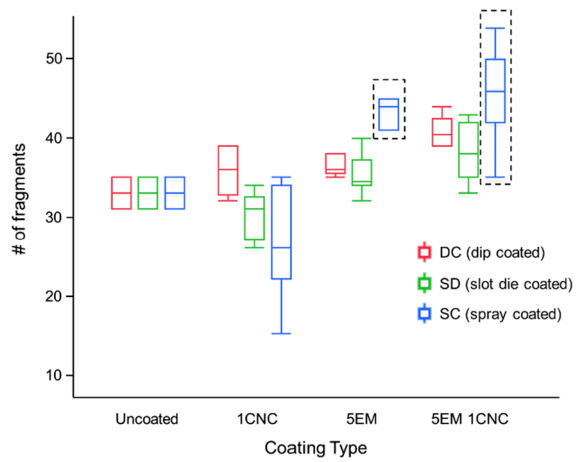

Fig. 9 SFFT fragment counts for all samples. Boxes represent the middle 50% of fragment count data. Box colors represent coating method. Dashed boxes represent statistically significant improvements over uncoated fibers

estimates of IFSS can vary widely across the literature. There is also a lack of consensus regarding the calculation of K', further increasing the variability of reported IFSS values (Hui et al. 1998). Furthermore, the Kelly-Tyson model is predicated on the assumption of elastic–plastic matrix behavior, which GF-epoxy composites do not conform to. For these reasons, Fig. 9 reports interfacial enhancement in terms of fragment count, a directly measurable value, since it is directly proportional to IFSS. They therefore

exhibit equivalent trends, and a higher number of fractures corresponds to a higher IFSS.

Results are grouped by coating composition and are further distinguished by application method based on the color of each plot. The boxes represent interquartile ranges, data between the 25th and 75th percentile of each sample set, and their height is a representation of data spread. The horizontal line inside each box represents median fragment count. The lines that extend beyond the top and bottom end of each box represent the maxima and minima of each dataset respectively. For the uncoated samples, the maxima and minima were identical to the 75th and 25th percentile values, hence the lack of extended lines. Data encompassed within dashed boxes represent statistically significant improvements over the uncoated control, as determined by the Tukey–Kramer pairwise comparison method in JMP Pro 15 (SAS Institute 2019).

Differences in average fragmentation due to coating type were observed. Depending on coating method, the 1CNC formulation (1 wt.% CNC) showed similar or lower fiber fragmentation compared to the as-received control GF. In contrast, the emulsion-based formulations, 5EM and 5EM 1CNC, yielded higher fiber fragmentation than the uncoated fibers for all coating methods. Furthermore, the 5EM 1CNC formulation outperformed the 5EM formulation in all cases, confirming the positive impact of CNCs at the fiber-matrix interphase.

Fiber fragmentation was also found to depend on coating method. DC outperformed SD and SC in the case of the 1CNC formulation. However, in the case of emulsion-based formulations (5EM and 5EM 1CNC), SD performed comparably to DC, and SC outperformed both other techniques. The Tukey–Kramer method was applied to understand if these differences in performance were statistically significant. Mean differences were calculated between all possible pairs of samples (see Table 3). If the mean difference for a given pair was not significant, a specific letter was assigned to both samples of that pair. This process was repeated for all possible sample pairs, meaning only the pairs with no overlapping letters were statistically different. The results reveal that emulsion-based SC samples exhibited an increase in average fragmentation over the control that was statistically significant at a 99% confidence interval. It is unlikely that these changes in fragmentation were caused by changes in the inherent mechanical properties of the fibers, as no forces or thermal treatments that could create surface defects were applied to the fibers during the fabrication of SFFT samples. Therefore, these trends are attributable to the coatings and their impact on interfacial adhesion.

Phenomena observed on coated fiber surfaces using SEM may help explain the trends in SFFT data. For example, the low performance of the 1CNC formulation was likely related to poor spreading on the fiber surface due to its low viscosity, as previously discussed. This led to thick coating deposits and inhomogeneity (see Fig. 5) that may have weakened the interphase. Similarly, the higher performance of SC relative to the other two methods may be related to morphological characteristics such as those shown in Figs. 3 and 4. The coating on the SC 5EM roving was visibly thinner and more homogeneous than the top side of the SD 5EM roving. Increasing magnification of the SC 5EM sample, particularly on visible patches of GF sizing, showed that the coating was well bonded to the GF surface. Cracks were also observed in these regions, but no delamination was observed. This suggests that the cracks may contribute to an increase in the surface area of the coating layer, potentially leading to greater interpenetration of the epoxy resin (Kim and Mai 1998). This may have resulted in stronger adhesion compared to DC and SD coated samples which exhibited no such cracking, though further analysis would be required to draw an explicit connection between cracking and IFSS.

The high scatter observed for SD and SC coated samples may have been caused by tearing of the coating layer as shown in Fig. 6. Coating damage exposes the underlying fiber, which forms a weak fiber-matrix interface based on the low fragment count for uncoated samples. This was likely the primary source of data spread for high-performance coatings such as SC 5EM 1CNC, as the best samples exhibited very high fracture counts while the worst were approximately on par with the control. This sample-to-sample inconsistency was not observed with DC fibers, substantiating the hypothesis that fiber separation was responsible for this phenomenon. However, it is important to note that this type of tearing is not likely to occur in industrial applications for two primary reasons. First, CNCs will ideally be incorporated into GF sizing when scaled, meaning the coatings described in this work would be applied

Table 3 Tukey–Kramer comparison of SFFT samples. Letters marked in red represent overlap with the uncoated control, and thus no statistically significant difference at a 99% confidence interval ($\alpha = 0.01$)

Level						Least squares mean (# of fragments)
SC 5EM 1CNC	A					45.3
SC 5EM	A	B				43.1
DC 5EM 1CNC	A	B	C			40.8
SD 5EM 1CNC	A	B	C			38.3
DC 5EM		B	C	D		36.6
DC 1CNC		B	C	D		35.8
SD 5EM			C	D		35.3
Uncoated			C	D	E	33.0
SD 1CNC				D	E	30.0
SC 1CNC					E	26.1

directly to single fibers during the manufacturing process. Second, full scale composites utilize unseparated chopped fiber rovings rather than separated single fibers with potentially damaged coatings, meaning average IFSS values in full scale composites are likely to be slightly higher than those reported in Fig. 9. Given that IFSS values for SD and SC emulsions were found to be favorable compared to DC emulsions despite this disadvantage, this finding provides further proof of the scalability of these coatings.

Optical characteristics of fiber fracture in SFFT samples

Cross-polarized optical microscopy was used to analyze the tested SFFT samples. Load applied during SFFT results in fiber fracture and deformation of the epoxy matrix surrounding the fracture location. This in turn results in residual stresses in the matrix that can be visually identified through bright birefringence patterns. A diagram of characteristic birefringence patterns and fiber fracture modes is provided in Fig. 10.

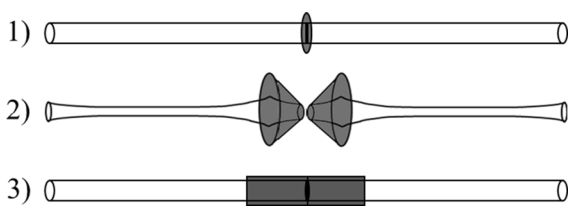

Fig. 10 Fracture modes in tested SFFT samples. (1) disk-shaped matrix crack (high strength); (2) double cone-shaped matrix crack (intermediate strength); (3) thin matrix crack and debonding (low strength)

Fracture type 1 has a thin, disk-shaped crack through the fiber that slightly propagates into the matrix. This represents a strong, rigid interface that does not debond during tensile testing, resulting in brittle fracture of the fiber. Fracture type 2 has a double cone shape that deflects at approximately a 45 degree angle into the matrix. This is characteristic of an intermediate interphase strength that exhibits moderate rigidity and toughness, resulting in more ductile fracture behavior. Fracture type 3 has a thin crack surrounded by bright birefringence and a long, dark debonding pattern. This indicates a weak interphase that debonds during tensile testing, resulting in sliding friction between the matrix and fiber. Representative fiber fractures observed in tested SFFT samples are shown in Fig. 11 and are labeled based on these fracture types.

The fracture types observed through optical microscopy largely reflect the trends previously described for SFFT. Samples with the lowest average fragmentation such as the uncoated fibers comprised mostly weak type 3 fractures surrounded by regions of extended debonding. The highest-performance coatings such as SC 5EM 1CNC instead predominantly exhibited stronger hybrid fracture types. Microscopy also helped identify which fibers exhibited damaged coating, as most SD and SC sample sets contained at least one coupon with exclusively type 3 fractures. This phenomenon was not observed in the DC samples, suggesting that coatings on some SD and SC fibers were damaged when single fibers were separated for SFFT. It is likely that the epoxy resin came into direct contact with the exposed sections of fiber in these samples, resulting in similar fracture patterns to uncoated fibers.

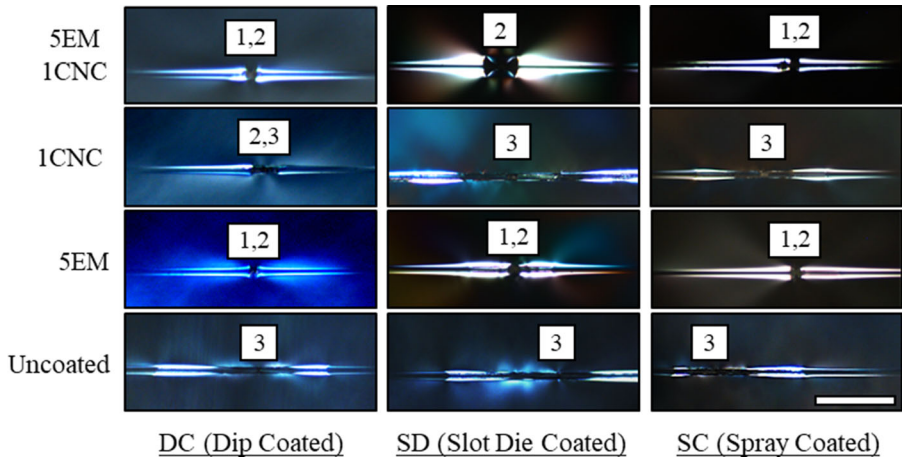

Fig. 11 Fracture modes of tensile-tested coupons containing uncoated fibers and fibers coated in 1CNC (1 wt.% CNC), 5EM (5 wt.% emulsion), and 5EM 1CNC (5 wt.% emulsion + 1 wt.% CNC) as observed by cross-polarized optical microscopy. Labels on fractures correspond to fracture modes illustrated in Fig. 10. Scale bars are 200 μm

The effect of CNCs was investigated by comparing samples coated with the 5EM and 5EM 1CNC formulations. SD and SC 5EM 1CNC yielded higher fracture counts than their 5EM counterparts while also exhibiting fewer type 3 fractures and less debonding, demonstrating that CNC reinforcement was achievable with both methods. This reinforcement may be related to an increase in coating surface area due to cracking as observed in Fig. 4, but it may have also been related to an increase in total coating mass upon the addition of CNCs. Mahmood et al. found that increased thicknesses of graphene oxide coatings on GFs led to higher IFSS in epoxy composites (Mahmood et al. 2016). This study also drew a tentative connection between fiber surface roughness and IFSS, substantiating the possibility that surface cracks in SC coatings may facilitate adhesion.

While the proportion of hybrid type 1/2 fractures increased upon adding CNCs, no pure type 1 fractures were observed. Stronger type 1 fractures would be expected to appear if CNCs greatly strengthened chemical interactions between the fiber and matrix. Zhao and Takeda demonstrated this phenomenon by coating GFs with an epoxy-compatible silane, which yielded more brittle fiber fracture behavior and higher IFSS compared to unreactive coatings (Zhao and Takeda 2000). These results imply that the role of CNCs in fiber-matrix adhesion is primarily related to influencing the physical characteristics of the coating layer rather than chemical interactions.

Limitations and optimization for slot die and spray coating

The SFFT results in Fig. 9 show that coatings produced by the SD and SC methods perform comparably to the laboratory scale DC method. However, these methods also present differences in operating conditions and resulting coating properties that are important to consider when determining which one to implement. SD performed slightly worse on average compared to SC in SFFT, but further analysis of the results suggests that the potential of SD has not been fully explored.

The coating solutions used in this work contained high amounts of water due to the hydrophilicity of CNCs, which typically aggregate heavily in non-aqueous solutions even after surface functionalization. This led to low solution viscosity and low coating bead stability, making it difficult to coat fibers evenly. To address this challenge, parameters such as slot die gap, solution flow rate, and carrier web velocity were set to low values. However, this was insufficient to overcome the instability of solutions with very high water content such as the 1CNC formulation. The use of a vacuum system presents a solution to this issue that may result in superior SD coating quality to what was observed in this work. In addition to improving coating bead stability, application of vacuum may also facilitate penetration of the coating formulation through gaps in the fiber roving, potentially leading to more uniform surface coverage. It may also lead to

increased production speeds by eliminating the need to lower the speed of the carrier web. SD coating can therefore offer significant benefits with respect to throughput, but realizing this potential requires modification to the experimental setup beyond what was explored in this study.

SC fibers produced the highest average IFSS values observed in this work. However, this result must be considered in context with the type of coating formulation used. In the case of the 1CNC formulation, SC failed to achieve uniform surface coverage, resulting in a low average SFFT fracture count with high error. This may have been caused by pressurization of the solution, which may have resulted in CNC aggregation. At scale, sedimentation of CNCs may exacerbate this issue, resulting in coatings with inconsistent CNC content. Extensive optimization of process variables including pressure and temperature therefore needs to be conducted separately for all coating types. Rail speed is also important to consider, as the mass of coating adsorbed onto the fiber surface was found to slightly decrease at higher speeds. Production rate is therefore another area of optimization to explore when considering the use of SC in fiber coating.

Conclusions

This study demonstrates the viability of using cellulose nanocrystals (CNCs) in glass fiber coatings to improve interfacial interactions in epoxy composites. Improvements previously achieved at lab scale are matched or exceeded herein using two industrially scalable methods. Key differences in morphology, structure, and loading are observed between all techniques, establishing an important connection between processing conditions and coating quality.

Slot die (SD) coating was found to perform nearly on par with dip coating (DC) in SFFT across all coating formulations used in this study. SEM analysis revealed that coating thickness differed on the top and bottom sides of SD coated glass fiber (GF) rovings due to direct exposure of the top side to the slot die head. The 1CNC formulation, a 1 wt.% aqueous solution of CNCs with methyl(triphenyl) phosphonium counterions, was particularly inhomogeneous, as it failed to spread evenly across the fiber surface. This was likely due to its high water content, which led to low viscosity and low stability of the coating bead deposited on the GF surface. Additionally, separation of single fibers for SFFT was found to induce coating damage that likely led to artificially low values of IFSS. The true performance of SD coating at scale is thus likely higher than what was reported in this work, and it could be further improved through more extensive process optimization. Application of vacuum can increase bead stability and facilitate penetration of coating through gaps in the roving. This would also enable increased carrier web speeds, making SD coating an appropriate choice for high throughput production.

Spray coating (SC) provided up to a 37% improvement in IFSS over uncoated fibers and up to an 18% improvement over fibers that were dip coated (DC) in equivalent coating formulations. As with SD formulations, these enhancements were achieved using epoxy-based emulsions, which outperformed purely water-based CNC suspensions. The higher performance of SC compared to DC and SD may have been related to differences in deposition mechanism. Deposition of discrete, micron-sized droplets in SC may have led to the formation of unique morphological characteristics such as surface cracks. These cracks may have increased the interfacial area between the coating layer and epoxy resin, thereby improving fiber-matrix interfacial interactions. Additionally, TGA revealed distinct decomposition peaks for SC coatings and broader, temperature-shifted peaks for SD coatings. This suggests that entrapment of CNCs within a network of emulsion polymers occurred less in SC samples, potentially allowing for more interactions between CNCs and the fiber and matrix. It was thus concluded that SC can yield high interfacial shear strengths, but appropriate selection of CNC dispersant and optimization of injection pressure profiles are necessary to maximize performance. The potential of using CNCs in GF coatings to improve GF-epoxy interfacial interactions, and thus the properties of GF composites, with industrially-relevant coating methods has been demonstrated.

Acknowledgements This research was funded by P^3Nano, the U.S. Endowment for Forestry and Communities, and the Renewable Bioproducts Institute at the Georgia Institute of Technology. The authors would like to thank Prof. Douglas M. Fox of American University for providing CNCs.

Authors' contributions This work was conceptualized by Ejaz Haque, Dorrin Jarrahbashi, Amir Asadi, Tequila Harris, Robert J. Moon, and Kyriaki Kalaitzidou. Supervision and funding acquisition were performed by Robert J. Moon and Kyriaki Kalaitzidou. Solution preparation, sample pre-characterization, mechanical testing, and data curation were performed by Ejaz Haque. Determination of slot die parameters and slot die coating were performed by Tae-Joong Jeong. Spray coating and jet image analysis and characterization were performed by Shadi Shariatnia. Draft manuscript preparation was performed by Ejaz Haque, Shadi Shariatnia, and Tae-Joong Jeong. Review and editing of final manuscript were performed by Ejaz Haque, Shadi Shariatnia, Tae-Joong Jeong, Dorrin Jarrahbashi, Amir Asadi, Tequila Harris, Robert J. Moon, and Kyriaki Kalaitzidou.

Availability of data and materials All data and materials support the claims herein and comply with field standards.

Code availability Not applicable.

Declarations

Conflict of interest The authors declare no conflict of interest.

References

Asadi A, Miller M, Moon RJ, Kalaitzidou K (2016) Improving the interfacial and mechanical properties of short glass fiber/epoxy composites by coating the glass fibers with cellulose nanocrystals. Express Polym Lett 10:587. https://doi.org/10.3144/expresspolymlett.2016.54

Asadi A, Miller M, Singh AV, Moon RJ, Kalaitzidou K (2017) Lightweight sheet molding compound (SMC) composites containing cellulose nanocrystals. Compos Struct 160:211–219. https://doi.org/10.1016/j.compstruct.2016.10.051

Cho W, Char K, Kwon S (2009) Thermally induced mesophase development in ethanesilica films via macromolecular templating approach. Macromol Res 17:697–702. https://doi.org/10.1007/bf03218930

de Assis CA et al (2017) Conversion economics of forest biomaterials: risk and financial analysis of CNC manufacturing. Biofuels Bioprod Biorefining. https://doi.org/10.1002/bbb.1782

Ding X, Fuller TF, Harris TA (2013) Predicting fluid penetration during slot die coating onto porous substrates. Chem Eng Sci 99:67–75. https://doi.org/10.1016/j.ces.2013.05.039

Ding X, Liu J, Harris TA (2016) A review of the operating limits in slot die coating processes. AIChE J 62:2508–2524. https://doi.org/10.1002/aic.15268

Fox DM et al (2016) Simultaneously tailoring surface energies and thermal stabilities of cellulose nanocrystals using ion exchange: effects on polymer composite properties for transportation, infrastructure, and renewable energy applications. ACS Appl Mater Interfaces 8:27270–27281. https://doi.org/10.1021/acsami.6b06083

Girotto C, Rand BP, Genoe J, Heremans P (2009) Exploring spray coating as a deposition technique for the fabrication of solution-processed solar cells. Sol Energy Mater Sol Cells 93:454–458. https://doi.org/10.1016/j.solmat.2008.11.052

Goffin A-L, Raquez J-M, Duquesne E, Siqueira G, Habibi Y, Dufresne A, Dubois P (2011) Poly (ε-caprolactone) based nanocomposites reinforced by surface-grafted cellulose nanowhiskers via extrusion processing: morphology, rheology, and thermo-mechanical properties. Polymer 52:1532–1538. https://doi.org/10.1016/j.polymer.2011.02.004

Goswami J, Haque E, Fox DM, Gilman JW, Holmes GA, Moon RJ, Kalaitzidou K (2019) The effect of cellulose nanocrystal coatings on the glass fiber–epoxy interphase. Materials 12:1951. https://doi.org/10.3390/ma12121951

Green R, Morfa A, Ferguson A, Kopidakis N, Rumbles G, Shaheen S (2008) Performance of bulk heterojunction photovoltaic devices prepared by airbrush spray deposition. Appl Phys Lett 92:17. https://doi.org/10.1063/1.2836267

Güler T, Demirci E, Yıldız AR, Yavuz U (2018) Lightweight design of an automobile hinge component using glass fiber polyamide composites. Mater Test 60:306–310. https://doi.org/10.3139/120.111152

Hösel M, Angmo D, Søndergaard RR, dos Reis Benatto GA, Carlé JE, Jørgensen M, Krebs FC (2014) High-volume processed, ITO-free superstrates and substrates for roll-to-roll development of organic electronics. Adv Sci 1:1400002. https://doi.org/10.1002/advs.201400002

Huber G, Hutai H, Klie W, Fischer W (1980) Bumper-support body consisting of glass-fiber-reinforced synthetic plastic material. US4208069A, USA

Hui C-Y, Phoenix SL, Shia D (1998) The single-filament-composite test: a new statistical theory for estimating the interfacial shear strength and Weibull parameters for fiber strength. Compos Sci Technol 57(12):1707–1725. https://doi.org/10.1016/S0266-3538(97)00103-6

Jeong T-J, Prasath R, Sitaraman SK, Harris TA (2020) Visualization of visualization of delamination in encapsulated flexible electronics fabricated using slot die coating. J Electron Mater 49:3332–3339. https://doi.org/10.1007/s11664-020-08065-2

Kelly A, Tyson WR (1965) Tensile properties of fibre-reinforced metals: copper/tungsten and copper/molybdenum. J Mech Phys Solids 13:329–350. https://doi.org/10.1016/0022-5096(65)90035-9

Kim J-K, Mai Y-W (1998) Engineered interfaces in fiber reinforced composites. Elsevier. https://doi.org/10.1016/b978-0-08-042695-2.x5000-3

Lagel M et al (2016) Automotive brake pads made with a bioresin matrix. Ind Crops Prod 85:372–381. https://doi.org/10.1016/j.indcrop.2015.12.090

Larsen-Olsen TT et al (2012) Simultaneous multilayer formation of the polymer solar cell stack using roll-to-roll double slot-die coating from water. Sol Energy Mater Sol Cells 97:22–27. https://doi.org/10.1016/j.solmat.2011.08.026

Lefebvre AH (1992) Twin-fluid atomization: Factors influencing mean drop size. Atomization Sprays 2:101–119. https://doi.org/10.1615/atomizspr.v2.i2.30

Lefebvre AH (1996) Some recent developments in twin-fluid atomization. Part Part Syst Charact 13:205–216. https://doi.org/10.1002/ppsc.19960130307

Mahmood H, Tripathi M, Pugno N, Pegoretti A (2016) Enhancement of interfacial adhesion in glass fiber/epoxy composites by electrophoretic deposition of graphene oxide on glass fibers. Compos Sci Technol 126:149–157. https://doi.org/10.1016/j.compscitech.2016.02.016

Moon RJ, Martini A, Nairn J, Simonsen J, Youngblood J (2011) Cellulose nanomaterials review: structure, properties and nanocomposites. Chem Soc Rev 40:3941–3994. https://doi.org/10.1039/c0cs00108b

Moon RJ, Schueneman GT, Simonsen J (2016) Overview of cellulose nanomaterials, their capabilities and applications. JOM 68:2383–2394. https://doi.org/10.1007/s11837-016-2018-7

Reichwein H-G, Langemeier P, Hasson T, Schendzielorz M (2010) Light, strong and economical–epoxy fiber-reinforced structures for automotive mass production. In: Proceeding of SPE automotive composites conference & exhibition. pp 1–20

SAS Institute (2019) Basic analysis. In: JMP® 15 Documentation Library. SAS Institute Inc., Cary, NC, US

Shariatnia S, Veldanda A, Obeidat S, Jarrahbashi D, Asadi A (2019) Atomization of cellulose nanocrystals aqueous suspensions in fused deposition modeling: a scalable technique to improve the strength of 3D printed polymers. Compos Part B: Eng 177:107291. https://doi.org/10.1016/j.compositesb.2019.107291

U.S. Department of Energy (2016) Quadrennial Technology Review 2015. Chapter 8: Advancing clean transportation and vehicle systems and technologies

Vak D, Kim S-S, Jo J, Oh S-H, Na S-I, Kim J, Kim D-Y (2007) Fabrication of organic bulk heterojunction solar cells by a spray deposition method for low-cost power generation. Appl Phys Lett 91:081102. https://doi.org/10.1063/1.2772766

Zhao FM, Takeda N (2000) Effect of interfacial adhesion and statistical fiber strength on tensile strength of unidirectional glass fiber/epoxy composites. Part I: experiment results. Compos Part A: Appl Sci Manuf 31:1203–1214. https://doi.org/10.1016/S1359-835X(00)00085-3